MIT Libraries | DSpace@MIT

MIT Open Access Articles

Forced Unfolding of Protein-Inspired Single-Chain Random Heteropolymers

Massachusetts Institute of Technology

Forced unfolding of protein-inspired single-chain random heteropolymers

Zexiang Han[†,§], Shayna L. Hilburg[†,§], Alfredo Alexander-Katz[†,]*

§These authors contributed equally.

[†]Department of Materials Science and Engineering, Massachusetts Institute of Technology, Cambridge, Massachusetts 02139, USA

*Correspondence: aalexand@mit.edu

KEYWORDS. Random heteropolymer (RHP), bioinspired, compactification, single-molecule mechanics, unfolding, topology, atomistic molecular dynamics, PEGylation

For Table of Contents use only

MMA: hydrophobic

OEGMA: mostly hydrophilic, high-molecular weight

EHMA: hydrophobic

SPMA: charged

Time
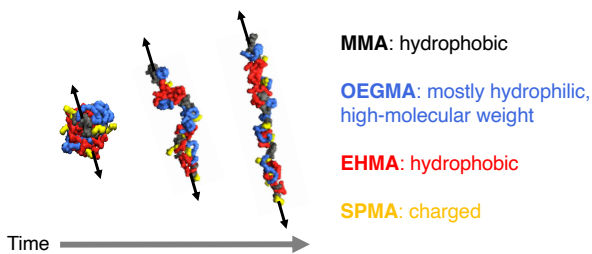
ABSTRACT

Synthetic random heteropolymers (RHPs) with high chemical heterogeneity can self-assemble into single-chain nanoparticles that exhibit features reminiscent of natural proteins, such as topological polymorphism. Using all-atom molecular dynamics simulations, this work investigates the structure and single-chain mechanical unfolding of a library of four-component RHPs in water, studying the effects of sequence, composition, configuration, and molecular weight. Results show that compactified RHPs can have highly dynamic unfolding behaviors which are dominated by complex side-chain interactions and prove markedly different from their homopolymer counterparts. For a given sequence and conformation, an RHP's backbone topology can strongly impact its unfolding response, hinting at the importance of topological design in the nanoscale mechanics of heteropolymers. In addition, we identify enthalpically-driven reconfiguration upon unfolding, observing a solvent-shielding protection mechanism similar to protein stabilization by PEGylation. This work provides the first computational evidence for the force-induced unfolding of protein-inspired multicomponent heteropolymers.

INTRODUCTION

The need to study single molecules stemmed from the desire to develop a more thorough understanding of the biophysics of proteins or nucleic acids when subjected to a form of stress. Compared to chemical or thermal stimuli, mechanical force serves as a distinct and orthogonal strategy to study single-molecule mechanics.[1] For folded proteins, highly heterogeneous mechanical responses are possible and proteins can undertake a range of mechanical (load-bearing or mechanosensing) and non-mechanical functions. One of the protein systems most commonly studied for its mechanical behavior is titin, a muscle protein exhibiting high elasticity. Force-

36 induced unfolding of a titin molecule reveals that its modular domains extend sequentially and

37 independently, where each domain unfolding event gives rise to one force peak (or rupture force),

38 attributable to the severing of a specific set of interstrand hydrogen bonds.[2–4] Titin, therefore, gives

39 rise to sawtooth patterns in force curves, which are also seen for other proteins for which secondary

40 and/or tertiary structure lead to defined domains, such as spectrin and ankyrin.[3,5,6] More generally,

41 force-extension profiles for protein unfolding have distinguishable features arising from the

42 sequence-defined structural interactions between amino acid side groups, such as the separation of

43 β-sheets and the uncoiling of α-helices. It naturally follows that, through examination of the

44 unfolding behavior, structural information can be gained. Through understanding the relative

45 forces required for dissociation of various portions of the proteins, insights into how the molecules

46 may respond when disrupted by an external force—be it mechanical, chemical, or thermal—are

47 provided.

48   While unfolding has been studied extensively for proteins and other natural biomacromolecules,

49 there exist fewer studies on the single-chain mechanics of synthetic macromolecules with

50 significant chemical complexity. Unfolding of hydrophobic homopolymer globules is well-

51 studied;[7–9] though, more complex collapsed synthetic polymers are less well characterized. A

52 subset of these complex macromolecules, which have been examined somewhat more thoroughly,

53 assemble through the incorporation of modularity and orthogonal chemistries.[10–12] Chung *et al*.

54 designed a modular polymer mimicking titin, exploiting the ability of the constituent monomer 2-

55 ureido-4-[1H]-pyrimidinone (UPy) to self-dimerize through hydrogen bonding.[10] Hosono *et al*.

56 reported the mechanical unfolding of a similarly designed single-chain nanoparticle (SCNP),

57 where the pendants within the chain can intramolecularly crosslink, leading to supramolecular self-

58 assembly or self-collapse.[11] As a result of such modularity, these two biomimetic polymers display

59 characteristic sawtooth patterns in their respective force-extension profiles and stepwise unfolding

60 pathways. Metal-π coordination chemistry has also been exploited for creating self-folding single-

61 chains in which rupturing of transient linkages can dissipate energy.[12] These examples rely on

62 specific, directional interactions. Fewer studies investigate the unfolding of globularly structured

63 SCNPs that assemble due to nonspecific interactions. Geissler and Shakhnovich were the first to

64 lay out an analytical treatment for the mechanical unfolding of general random heteropolymers

65 (RHPs).[13,14] They proposed that, during heteropolymer unfolding, there will likely have a pearl-

66 necklace-shaped intermediate. The existence of this morphology can be ascribed to solvation

67 effects, where hydrophilic regions are prone to extend upon unfolding whilst hydrophobic regions

68 remain collapsed and compact to minimize solvent exposure, forming "pearls". We expect that the

69 stability of pearl-necklace morphologies will be dependent on the exact sequence. For instance, a

70 heteropolymer where hydrophobic clusters are periodically spaced within the chain will likely

71 experience this necklace-like intermediate compared to one that is completely random. While

72 insights can be gained from these studies, they lack chemical detail which we have previously

73 demonstrated to be vital to understanding specific random heteropolymer assembly.[15]

74   Of the existing reports on the forced unfolding of macromolecules, most work is experimentally

75 enabled by a suite of single-molecule force spectroscopy techniques including atomic force

76 microscopy, optical tweezers, and magnetic tweezers.[16,17] However, these techniques fail to help

77 visualize the purported unfolding events. An area for exploration is *in situ* imaging of single

78 molecules during mechanical unfolding for multimodal analysis. Both single-molecule

79 fluorescence imaging and *in situ* liquid-cell electron microscopy may be possible candidates,

80 though their developments are only in their infancy.[18,19] *In silico* methods modeling single-

81 molecule nanomechanics are therefore an attractive alternative, capable of providing mechanistic

82   insights. Common computational methods to study single-molecule mechanical response include

83   all-atom steered molecular dynamics (SMD)[2,20,21], coarse-grained Brownian dynamics[7], and Monte

84   Carlo simulations[22]. Among these, all-atom SMD is particularly favored for studying the forced

85   unfolding of chemically heterogenous biomolecules due to the atomistic resolution that proves

86   essential to capturing their conformational flexibility and diversity. Atomistic modeling also

87   explicitly includes polar interactions with water molecules, which is particularly useful in

88   modeling the unique amphiphilic behavior of polyethylene glycol (PEG).[23,24] One evident

89   limitation of atomistic SMD and similar computational techniques is the difficulty to access micro-

90   to millisecond timescales due to a correspondingly high computational cost. As a result, the typical

91   pulling speed employed in SMD lies in the range of $10 - 100$ Å ns^{-1} (Table S1), which is six to

92   seven magnitudes faster compared to those used in experimental methods.[20–22,25–31] Due to the

93   orders-of-magnitude difference in pulling velocities, SMD results often overestimate force peak

94   values compared to empirical values. In spite of this, it is still common to correlate experimental

95   findings with simulations in order to gain mechanistic insights into the unfolding events and

96   elucidate unfolding pathway(s), and there is typically a satisfactory qualitative agreement between

97   simulations and experiments.[21,32]

98   Overall, single-molecule mechanics is of paramount importance for understanding the internal

99   structure and response to external forces of polymeric chains. Using a recently reported RHP

100   system as an example[33], this work characterizes the single-chain mechanical response of a highly

101   chemically heterogeneous polymer system. Xu and colleagues took inspiration from natural

102   proteins and rationally designed methacrylate-based statistical RHPs, which serve as a novel class

103   of biomimetic materials.[33] These four-component RHPs incorporate methyl methacrylate (MMA),

104   oligo(ethylene glycol) methacrylate (OEGMA), 2-ethylhexyl methacrylate (EHMA), and 3-

105   sulfopropyl methacrylate (SPMA) (Figure 1A). The monomer selections are intended to leverage

106   varied amphiphilicity and polarity to recapitulate the heterogeneity of native protein chains and

107   resulting surfaces.[15] Such a design differs from many past SCNPs, which rely on intramolecular

108   crosslinking strategies, and more closely resembles the self-assembly of natural

109   biomacromolecules.[10–12] The RHPs can mimic protein functions and interface favorably with

110   proteins, finding applications as synthetic alternatives to molecular chaperones to stabilize proteins

111   in non-native environments[33,34], as mimics of transmembrane proteins to facilitate selective proton

112   transport[35], and as enzyme protectants to facilitate the degradation of commodity plastics[36].

113   Atomistic modeling of these RHPs in water revealed that while the RHP structures are not

114   sequence-defined, some structural motifs emerge in their collapsed form and a variety of

115   assemblies are possible.[15] We also showed that the RHPs possess minimal backbone mobility in

116   water; however, experiments have demonstrated that the RHPs can interact with other

117   biomacromolecules and small molecules, suggesting that external stimuli could provide the driving

118   force to at least partially unfold portions of the molecules. Herein, we perform all-atom MD

119   simulations to characterize RHPs with degrees of polymerization of 20 and 50 (referred to herein

120   as 20mers and 50mers, respectively) in water. Sequences of various compositions and

121   arrangements of the four methacrylate-based components are investigated (Figure 1A) using SMD

122   to study their unfolding (Figure 1B). To the best of our knowledge, no prior work has been

123   performed to investigate the unfolding behavior of synthetic heteropolymers as chemically

124   complex as the four-component amphiphilic RHPs presented here. Aforementioned theoretical

125   treatments of heteropolymers often neglect atomistic details and cannot accurately capture the

126   conformational complexity of chemically heterogeneous polymers.[13,14,37] Thus, our investigation

127   of this bioinspired RHP system not only adds a different chemistry to the current portfolio of forced

128   unfolding of synthetic heteropolymers, but also affords a library of polymer sequences for

129   investigation. Moreover, by understanding how the RHP responds to a tensile force stimulus, we

130   can appreciate what would likely be required for backbone remodeling to take place and gain

131   insights into internal structural dynamics and stability of the RHPs in water.

132
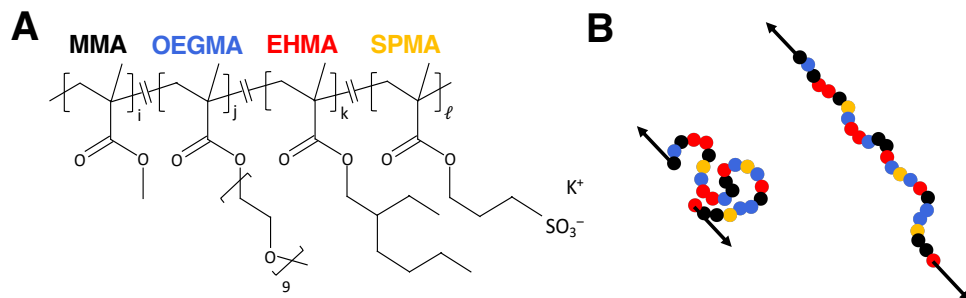
133

134   **Figure 1. Protein-inspired RHP studied in this work.** (A) RHP chemical structure. Monomers

135   are color-coded as follows: MMA in black, OEGMA in blue, EHMA in red, and SPMA in yellow.

136   (B) Schematic showing the forced unfolding of an RHP from its collapsed state.

137

138   **RESULTS & DISCUSSION**

139   *RHP chain compactification*

140   The self-assembly of explicitly solvated single-chain heteropolymers is studied, with sequence

141   schematics of all 20mer and 50mer RHPs investigated in this work provided in Figure S1.

142   Similarly to 100mer RHPs of the same chemistry[15], individual 20mer and 50mer RHP sequences

143   can self-assemble into multiple conformational states. For a given chain, 10 annealing cycles lead

144   to the sampling of 10 distinct conformers, each with unique topological organization in the

145   backbone (Figures S2 and S3). Such topological heterogeneity has also been observed in certain

146   intrinsically disordered proteins as well as synthetic SCNPs of similar sizes, alluding to the rich

7

147 conformational energy landscape of these comparable systems.[38,39] Standard deviation of the

148 absolute value of backbone dihedral angles is used as a measure for backbone mobility over the

149 relevant timescale. By this measure, the ten conformational states sampled are believed to be

150 metastable in nature as the backbones minimally change, as illustrated by the small standard

151 deviation of |dihedral angles| over 40 ns for the equilibrated system in water (Figure 2A). For both

152 20mers and 50mers, the ends of the RHPs are, as expected by the configurational entropy of linear

153 polymer chains, more mobile than the middle.

154   Mobility comparisons between RHPs of different molecular weights show that both the middle

155 and end segments of the 50mers reconfigure less than their counterparts in the shorter polymers in

156 unbiased MD simulations. From this trend, we can imply that the longer polymers are more

157 compact, impeding backbone rearrangement. This is confirmed by Figure 2B, whereby an analog

158 for density (polymer mass divided by the radius of gyration, R_g, cubed) generally increases with

159 molecular weight. One notable exception is sequence 19, which shows a decrease in density when

160 comparing its 20 and 50mer lengths. This result stems from the anion-anion repulsion of the SPMA

161 monomers, of which sequence 19 has the highest proportion investigated in this work, leading to

162 polyelectrolyte-like behavior. We would not expect an RHP with a high negative charge to

163 compactify into a globular morphology; instead, an amphiphilic polymer with a high net charge

164 would adopt a more extended conformation, giving rise to a lower density.[40,41] The typical RHP

165 trend, however, shows compactification as well as a narrowing of the range of densities between

166 sequence conformations as molecular weight increases. The narrower range of density values

167 stems from the greater similarity in R_g values for 50mers, as despite different backbone topologies,

168 configurations all led to compact globules. For 20mers, some sequence conformations formed

169 denser assemblies while others remained extended, indicating a stochastic compactification with

close energetic competition between the entropic cost of limiting mobility in a compact globule

and the enthalpic surface energy penalty of exposing hydrophobic monomers to the aqueous

environment. As smaller oligomers, the RHPs will be soluble, because even MMA, one of the

more hydrophobic monomers in our polymer, is soluble at extremely low degrees of

polymerization.[42] Therefore, based on the simulation results, most compositions of RHPs with

degree of polymerization of 20 appear to be near the energetic cliff for compact globule formation,

while 50mers in the same windows are nearly all compact and more uniform in density.
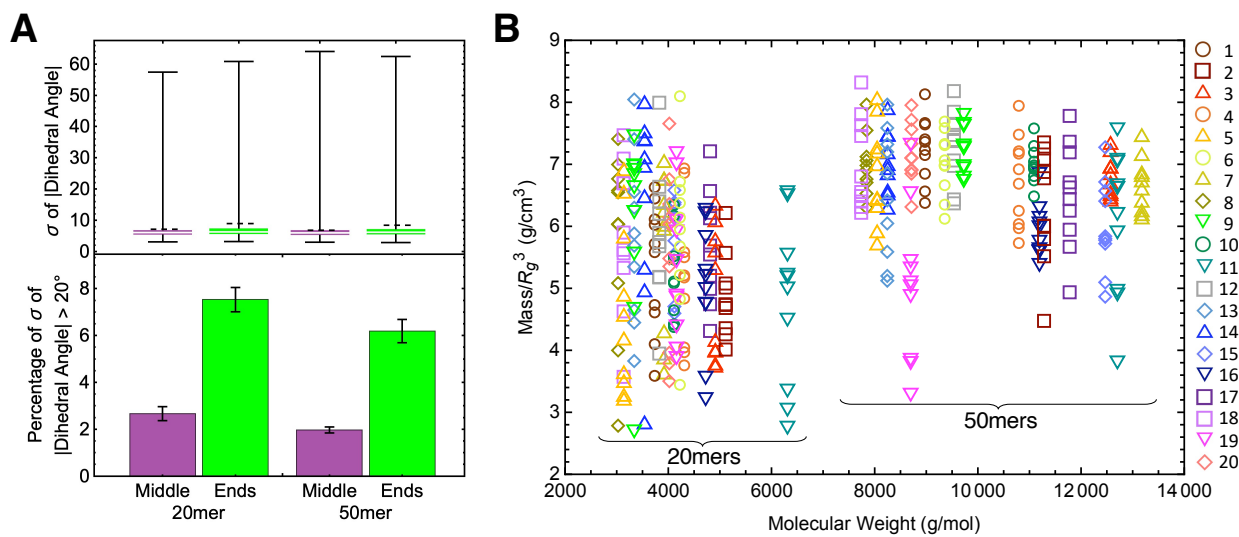
Figure 2. RHP chain mobility and its compactification. (A) (Top) Box-and-whiskers plot of the
raw standard deviation σ of |dihedral angle| for each conformation from the 40 ns of equilibration,
for all 20mer and 50mer RHP sequences and conformations, respectively. Dashed lines represent
the mean. The "ends" refer to the 8 dihedral angles from the 5 monomers on each end (thus in total
16 dihedrals) regardless of the RHP length; the remaining dihedrals are in the "middle" of the
RHP. (Bottom) Percentage of σ of |dihedral angle| values greater than 20° for RHP ends vs. middle
over the 40 ns of equilibration. Error bars represent standard error around the mean for the 200

186   conformations (20 sequences with 10 conformations each). (B) Density analog for all 20mer and

187   50mer sequence conformations *versus* molecular weight (MW). The density analog in g cm^{-3} is

188   calculated as MW × Avogadro's number N_A / R_g^3, with appropriate unit conversions. RHPs

189   generally show compactification as molecular weight increases, with several exceptions explained

190   in text. Corresponding sequence schematics are given in Figure S1.

191

192   ***RHP responses to force-induced unfolding***

193   For a selection of polymer sequences, five independent replicates were studied under an applied

194   tensile force to induce unfolding at a constant rate of 1 Å ns^{-1}. To ensure a sufficiently slow pulling

195   rate for our RHP system, we perform *in silico* stress-relaxation experiments on one 50mer RHP,

196   sequence 12. Snapshots during the unfolding simulation were extracted every 10 ns (*i.e.,* 0 ns, 10

197   ns, 20 ns, … 100 ns), and each is then stress-relaxed by maintaining the end-to-end distance

198   restraint and allowing the chain to equilibrate for 20 ns while monitoring for relaxation behaviors

199   (Figure 3A). The backbone dihedrals show only a few changes upon stress relaxation for

200   essentially all unfolding intermediates (Figure 3B and S4), indicating relatively insignificant

201   backbone reconfiguration. In addition, the magnitudes of changes in the dihedral angles for the

202   partially unfolded structures are not far from those for the initial equilibrated structure (Figure 3C,

203   top), and the mobility of the backbone of the structural intermediates remains low (Figure 3C,

204   bottom). This suggests that the initial structural snapshots do not deviate much from their stress-

205   relaxed states. We also see minimal reconfiguration within the side-chains, which are generally

206   more mobile than the backbone, during the 20-ns stress relaxation. In fact, RHP solvation, which

207   is dominated by side-chain/water interactions, remains nearly constant over the course of the

208   stress-relaxation (Figures 3D and S5), indicating extremely rapid water solvation. Provided this

209 minimal RHP reconfiguration, the pulling rate employed is sufficiently slow for gaining

210 mechanistic insights into the RHP behavior upon unfolding. Our results show that the RHPs are in

211 a pseudo-equilibrium regime during force-induced unfolding, and the unfolding observed through

212 our procedures is likely a low energy pathway.

213

214
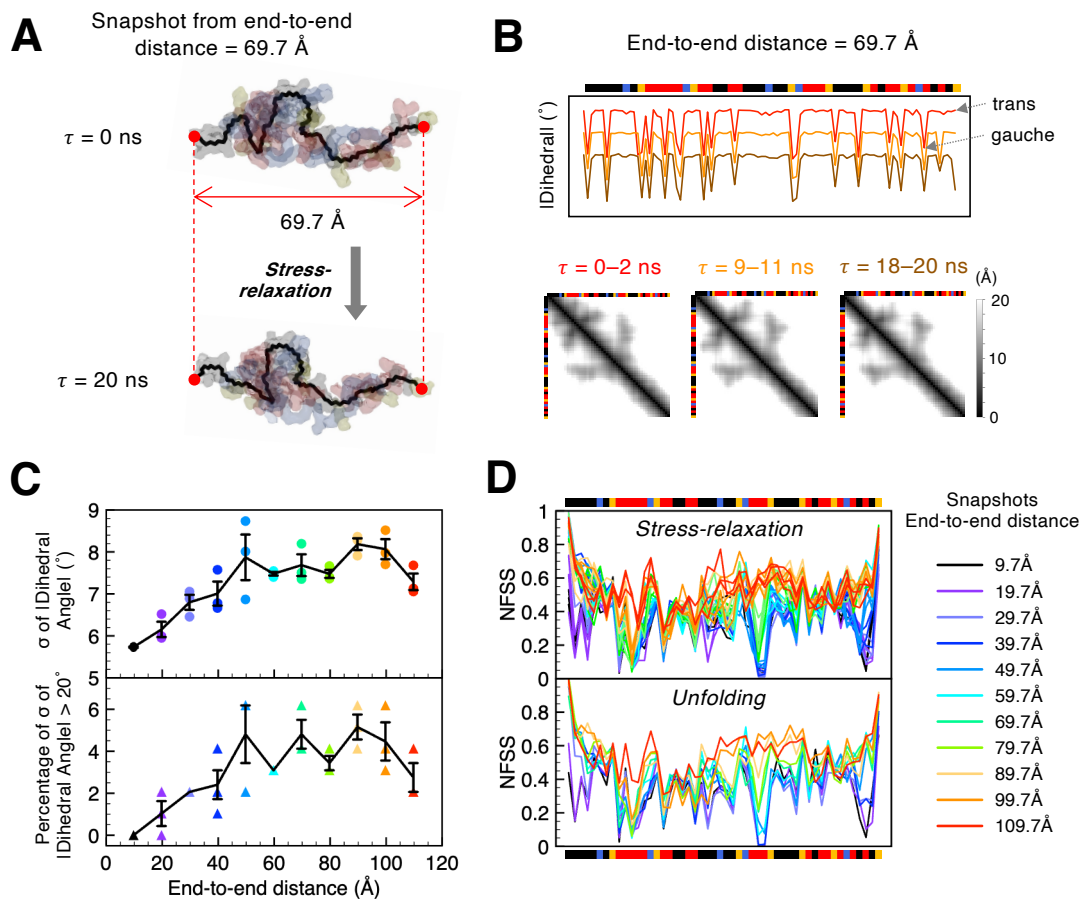
Figure 3. Insignificant backbone and side-chain remodeling upon RHP stress-relaxation.
Results shown here are for 50mer RHP sequence 12 conformation 8. (A) Illustration of the stress-relaxation protocol on an RHP snapshot from unfolding time $t = 60$ ns. End-to-end distance is maintained constant during the 20-ns stress-relaxation. Note that the stress-relaxation time is represented by τ in order to differentiate from the unfolding time t. (B) Stress-relaxation responses

220   in the backbone of the snapshot RHP structure from $t = 60$ ns. Time evolution of dihedral plots,

221   each averaged over 2 ns. Representative time-averaged C_α-based contact map evolution,

222   confirming insignificant remodeling in the RHP backbone. (C) (Top) Average standard deviation

223   σ of the absolute value of all 97 dihedral angles throughout the 20-ns stress-relaxation against

224   different unfolding intermediates. The end-to-end distances correspond to the extracted RHP

225   snapshots from time $t = 0$ ns to $t = 100$ ns during its unfolding process. Each data point is from one

226   independent stress-relaxation simulation. (Bottom) Average number of dihedrals with a σ greater

227   than 20°. Error bars represent standard errors around the mean. (D) Normalized first solvation shell

228   (NFSS) along the sequence for different unfolding intermediates for (top) stress-relaxation and

229   (bottom) mechanical unfolding, showing minimal change in solvation after RHP stress-relaxation.

230   The corresponding time points for each of the end-to-end distances are time-averaged: for stress-

231   relaxation, they refer to the average NFSS for the last 2 ns of the stress-relaxation, and data from

232   three replicates are shown. For unfolding, they refer to the average NFSS at the corresponding

233   unfolding times t (for example, 9.7 Å means averaging across $t = 0$–2 ns, and 19.7 Å means

234   averaging across $t = 9$–11 ns).

235

236   Force curves are recorded from each constant-velocity unfolding replicate using SMD. There

237   thus exist three possible unfolding events which can have varying extent of overlap: (i) concerted

238   breakage of a set of noncovalent interactions, which require a high force/energy; (ii) breakage of

239   noncovalent interactions one by one, or "unzipping", which require a lower unfolding force that

240   spans over a longer range of extension, as well as (iii) breakage of a set of dynamically evolving

241   intramolecular interactions, whose force curve features will likely be diffuse or stochastic and

242   more difficult to interpret. For our RHPs, visual inspection of the unfolding trajectories does not

243   establish an unambiguous correlation between force curve features – peaks or plateaus – with

244   molecular snapshots. Examination of individual unfolding replicates of a given RHP conformer

245   shows that side-chains have highly dynamic interactions that vary across the five replicates. For

246   example, the solvent-accessible surface area (SASA) evolution over time exhibits different

247   behaviors across the five replicates, even though some force curves exhibit very similar features

248   for a given 20mer RHP (Figure S8). Variable pathways for backbone restructuring are also

249   observed through the evolution of dihedral angles. We can hence suspect that force curve features

250   are a result of a combination of topological variations in the polymer backbone as well as side-

251   chain interactions rather than a one-to-one correlation of a particular force peak to the

252   disassociation of two moieties. Though each RHP sequence conformation replicate has a unique

253   unfolding trajectory, they share commonalities reflected in the averaged force curve from which

254   we can gain insight to the polymer assembly.

255   Since the coil-to-globule transition for hydrophobic homopolymers is well studied,[43] the force

256   responses for unfolding collapsed homopolymers of chemistries relevant to our RHPs – namely,

257   PMMA and PEHMA – are studied as controls (Figure 4). The unfolding force is rate-dependent in

258   polymeric systems; therefore, the magnitude of the unfolding forces recorded in SMD simulations

259   will be higher than measured by experimental single-molecule techniques which operate at a

260   pulling velocity orders of magnitudes lower.[20] For PMMA, an initial force peak is present in several

261   of the simulations, and is attributable to the disruption of intrachain dipole-dipole interactions due

262   to PMMA's directional and polar side group. Once the dipole-dipole self-packing interactions are

263   disrupted upon initial unfolding, polar side groups of PMMA can become solvated with water, and

264   it only requires minimal (near-zero) force to unfold the chain further, resulting in a force curve

265   traditionally consistent with PMMA's glassy nature. For PEHMA homopolymers, their force

curves exhibit more features and show a greater variability between the unfolding replicates compared to that of PMMA, demonstrating highly dynamic side-chain interactions, as seen by visual inspection in the simulation trajectories. The averaged force curve for PEHMA$_{50}$ also displays a characteristic plateau-like behavior at a non-zero force which is ascribed to hydrophobic hydration.[9]
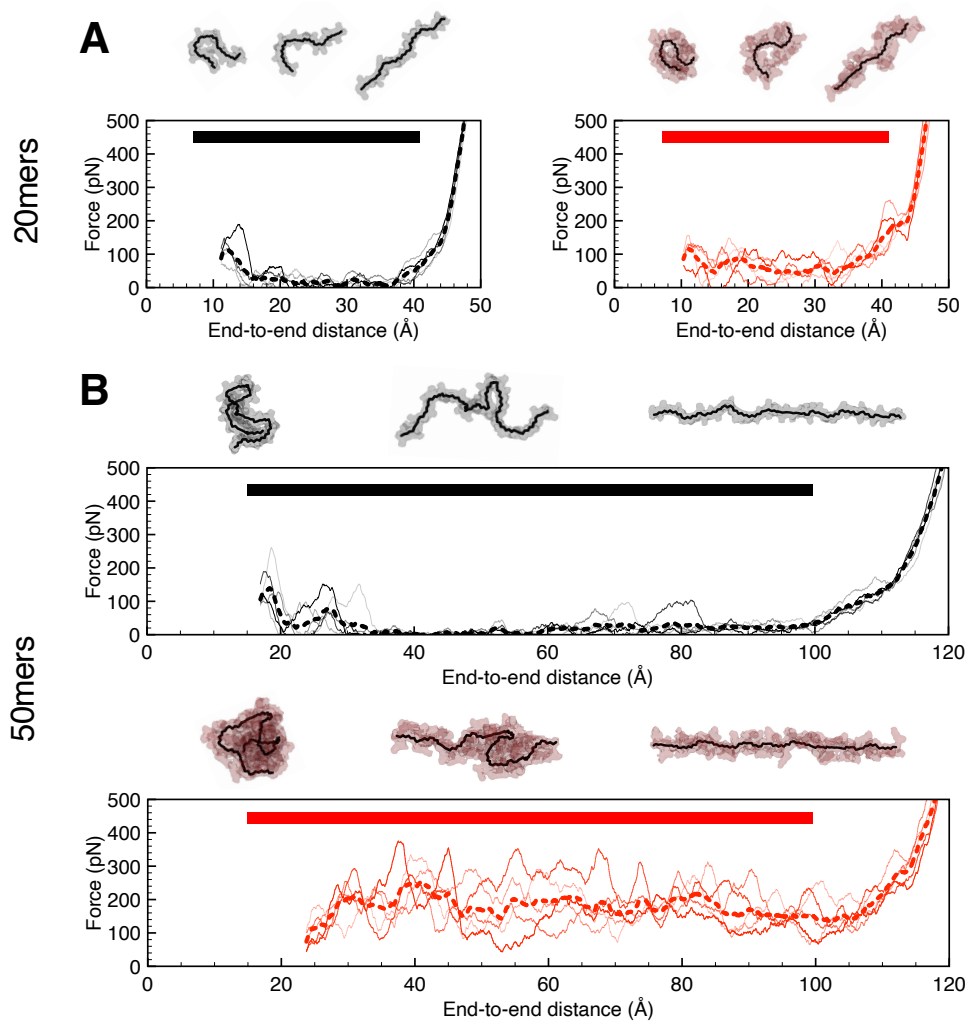

Figure 4. Unfolding force curves of hydrophobic homopolymers. Force curves for (A) 20mer and (B) 50mer homopolymers PMMA (black) and PEHMA (red) are based on moving averages over 2-Å intervals. Shown are the data from five independent unfolding simulation replicates in

276 different shades of the same color, and the average is given in a thicker dotted line. Example

277 snapshots of initial, intermediate (midpoint), and final conformations of the polymer during

278 unfolding are provided, where side-chains have been rendered semi-translucent to highlight

279 polymer C–C backbone topologies.

280

281   For the multicomponent RHPs, their equilibrated structures are often stabilized by the

282 hydrophobic attraction between EHMA-EHMA side-chains. Some sequences also have

283 conformations stabilized by OEGMA-OEGMA interactions or by a mixture of EHMA and

284 OEGMA interactions, depending on the monomer availability within the chain. Compared to their

285 homopolymer counterparts, 20mer and 50mer RHPs display more varied mechanical responses

286 (Figures 5, S6, and S7). In terms of force curve features, some 20mer RHPs exhibit clear and

287 pronounced force peaks across five replicates, some exhibit a plateau behavior, and some can have

288 more frequent force peaks than others. This demonstrates that the RHP system has an extremely

289 rich energy landscape which can result in vastly different single-chain mechanical responses, even

290 for identical sequences as short as 20 monomers in length. Similarly, force curves of 50mer RHPs

291 also display varying extents of force peaks and plateaus depending on the exact sequence and

292 conformation of the chain. The diverse force curves for unfolding RHPs are distinct from those

293 observed for biological heteropolymers such as proteins or nucleic acids of similar sizes. For

294 example, the unfolding force curve of single-stranded DNA hairpin structures of 55 bases in size

295 reveals a characteristic "rip" feature, indicative of disruption of the hydrogen bonding.[44] This

296 disparity arises from three major design differences between RHPs and biopolymers (*e.g.* proteins

297 or nucleic acids). First, RHPs do not have intramolecular hydrogen bonding that proves

298 fundamental for the secondary structural formation in proteins. Secondly, RHPs possess several

bulkier and longer side-chains compared to native amino acids that make up proteins (or nucleotides that make up nucleic acids), giving rise to unfolding behavior dominated by side-chain interactions and reconfiguration. Thirdly, RHPs have a racemic mixture of monomers with randomly assigned chiralities – that is, our RHPs are heterochiral – whereas proteins and nucleic acids are intrinsically homochiral. As a result, no characteristic rupture forces from the breakage of specific ordered interactions are observed in RHPs.
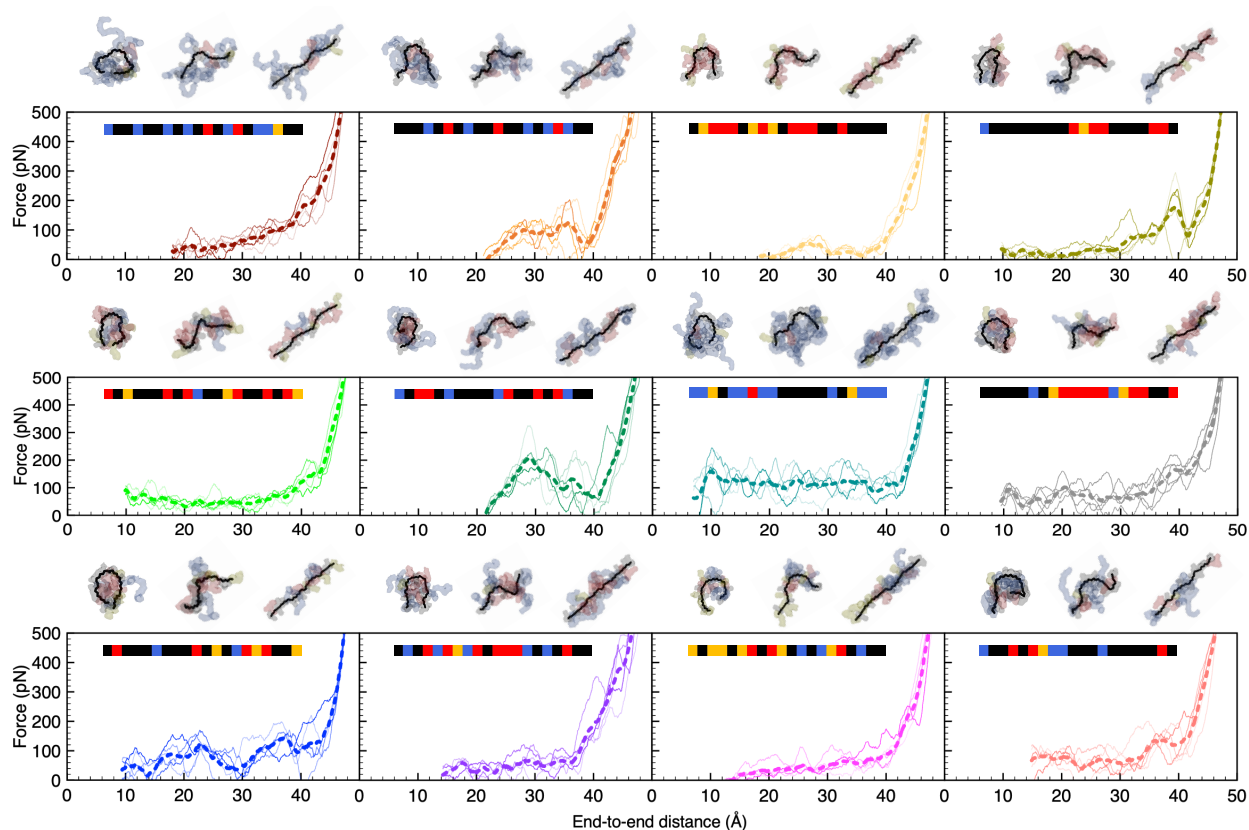
Figure 5. RHPs show varied responses to force-induced unfolding. Shown here are the force curves for the unfolding of selected 20mer RHPs with their unfolding trajectory snapshots (initial, intermediate, and final conformations). An exhaustive overview of the unfolding force curves of all 20mer and 50mer RHPs studied are provided in Figures S6 and S7, respectively.

16

311

Monitoring the unfolding pathway and behavior of individual RHP sequences

312

313   The unfolding behavior of an RHP is investigated in detail by monitoring the time evolution of

314   dihedral angles and intramolecular contacts to understand backbone restructuring and elucidate the

315   unfolding events. Here, we detail the unfolding pathway of a molten globular 50mer RHP,

316   sequence 12 conformation 8. As with many 50mer RHPs, the mechanical unfolding of this RHP

317   is mostly driven by the dissociation of the hydrophobic core formed by EHMA-EHMA interactions

318   (Figures 6 and S9). During the first 30–40 ns of unfolding, there are few apparent dihedral angle

319   transitions except for the two ends. In fact, the internal structure of the RHP is well preserved

320   during the initial mechanical perturbance, confirmed by the preservation of contacts from pulling

321   time $t = 1$ ns to 30 ns (Figure 6C). Therefore, conformational changes are possibly mediated by

322   the extension of the two chain ends which possess higher mobility as demonstrated by unbiased

323   MD simulations and by diffuse, small changes throughout the entire chain in order to enable the

324   initial increase in end-to-end distance. On a morphological level, the globule becomes somewhat

325   distorted under the applied force. From $t = 50$ to 60 ns, the chain undergoes segmental separation

326   where the EHMA hydrophobic core dissociates into two separate, smaller EHMA-stabilized cores.

327   Examining the dihedral evolution, this is believed to be mediated by the extension of the MMA

328   block (highlighted by red boxes in Figure 6C), as indicated by the distinct gauche to trans angle

329   transition. This pearl-like intermediate is similar in shape to that predicted by theory[13,14]; however,

330   in the case of this specific RHP, a hydrophobic MMA block instead of a hydrophilic cluster unfolds

331   first. Upon segmental separation, the extensions of the two smaller units unfold sequentially, where

332   the longer EHMA segment near the beginning of the sequence has persistent hydrophobic

333   interactions until $t = 90$ ns and unfolds last (highlighted by green boxes in Figure 6C). Overall,

334 during the latter stages of the unfolding pathway (after $t = 50$ ns), EHMA side-chains, which

335 previously had longer range hydrophobic interactions, have an increased number of local

336 interactions due to their physical proximity within the sequence, giving rise to the emergence of

337 some gauche angles in the more extended conformation. Analyses on the four other replicates of

338 this RHP sequence and conformation also show relatively similar unfolding pathways; however,

339 the segmental separation can take place at a different MMA block *via* its extension (Figure S10).

340 This suggests that the MMA blocks can behave as a hinge, such as the α-helical linker in spectrin[5],

341 to mediate or propagate unfolding. This is supported by our finding that PMMA homopolymers

342 require minimal force to unfold, leading MMA blocks within an RHP to be more amenable to

343 reconfigure during unfolding. Nevertheless, it should be noted that MMA blocks do not always

344 behave in this manner in the sequences investigated, and there are a myriad of complex interactions

345 that would allow alternative unfolding pathways to exist, making this phenomenon highly

346 sequence- and conformation-specific.

347

348

18
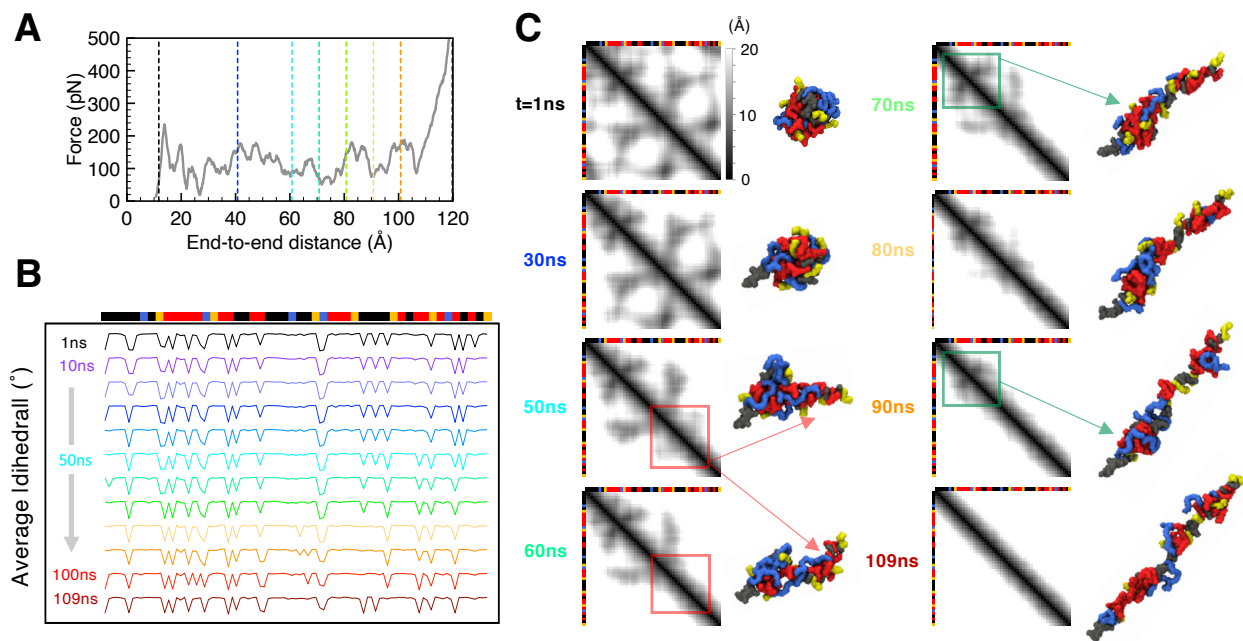
Figure 6. Monitoring the unfolding pathway of a 50mer RHP. This particular RHP corresponds to sequence 12 conformation 8, and results from a representative unfolding replicate is shown here. (A) Unfolding force curve. Vertical dotted lines indicate specific time points of interest. (B) Backbone dihedral angle evolution for the entire unfolding process of this RHP. (C) Selected 2-ns-time-averaged C_α-based contact maps. Red/green boxes highlight regions of interest. Corresponding VMD snapshots of the RHP are also shown to visualize the unfolding events. The unfolding trajectory showing the unfolding intermediates per every 10 ns is provided in Figure S9. The unfolding trajectory of this RHP visualized in VMD is provided in Supporting Information Movie S1.

Another finding observed in the study of sequence 12 conformation 8, as well as several other compositions and configurations, is that upon RHP unfolding, OEGMA side-chains wrap around the surface of the main RHP chain. Throughout the unfolding trajectory, different OEGMA side-chains preferentially interact with hydrophobic regions, as highlighted in Figure 7, where darker regions in the contact maps calculated from side-chain centers of mass denote the physical proximity between the side groups of each monomer. Since the contact maps are time-averaged over 2 ns, the residues have significant residence times rather than being coincidental instantaneous occurrences. OEGMA, shown to be amphiphilic in nature[15,45] and whose side-chains possess high conformational flexibility, can establish a favorable interface between the hydrophobic monomers and the water molecules, serving as a possible protection mechanism *via* solvent shielding. To obtain direct, quantitative evidence of OEGMA wrapping, separation distances between the tail atoms of OEGMA and EHMA residues are computed and plotted against time for all possible OEGMA/EHMA pairs in the RHP sequence (Figure 7C). Small separation

19

372 distances between the two tail atoms can arise either from sequence effects due to mere geometric

373 proximity between covalently bound monomers within the chain or from the wrapping phenomena

374 we intend to capture. To decouple the two effects, EHMA monomers have been grouped into four

375 groups based on their positions in this particular sequence. The fourth OEGMA monomer,

376 highlighted in magenta, is actively involved in the wrapping process, as observed from the

377 nonmonotonic time-dependence in the separation-distance curves with multiple regions of EHMA

378 (Figure 7). OEGMA-EHMA distance curves for the other OEGMA residues do not manifest the

379 same extent of wrapping (Figure S11). Moreover, this wrapping phenomenon has been observed

380 for numerous 20mer and 50mer RHPs studied, establishing its relative generality. Whilst this

381 observation is novel for our particular chemistry, the solvent-shielding phenomenon is reminiscent

382 of previously studied interactions between PEG — which makes up the long OEGMA side-chain

383 — and biomolecules. Conjugation of proteins with PEG chains (PEGylation) and similar

384 molecular brushes is a method to enhance the thermal and mechanical stability of certain proteins

385 using covalent modifications.[46–48] While comprehensive studies providing mechanistic insights are

386 limited, DeBenedictis *et al*. report that PEG chains can wrap around an α-helical protein and shield

387 water molecules from attacking the hydrogen bonds, delaying the unfolding process.[49] Moreover,

388 they show that the PEG chains disproportionately favor hydrophobic and charged residues,

389 phenomenologically similar to the OEGMA wrapping in our system.

390

391
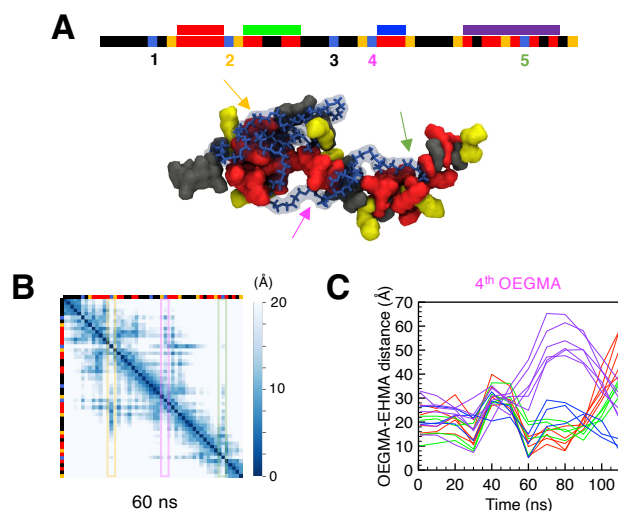
Figure 7. OEGMA side-chain wrapping is observed during RHP unfolding. (A) RHP sequence schematic (sequence 12) and a structural snapshot at pulling time $t = 50$ ns. EHMA monomers within this sequence can be approximately grouped into four sets, color-coded in red, lime green, blue, and purple. OEGMA monomers are numbered and color-coded as shown in the sequence. The same color-coding is used to indicate OEGMA monomers in the snapshot, showing OEGMA wrapping around hydrophobic EHMA and charged SPMA residues. The OEGMA side-chains have been rendered semi-translucent and water has been excluded for ease of visualization. (B) A time-averaged side-chain-based contact map showing preferential interactions of some OEGMA side-chains with hydrophobic residues. (C) Time evolution of tail-atom separation distances for the second OEGMA monomer to the other EHMA monomers based on 2-ns-time-averaged tail-atom contact map data. Therefore, each line in the plot corresponds to the tail-atom distance of one particular OEGMA/EHMA pair. Similar plots for the other OEGMA monomers can be found in Figure S11.

405

406   Differently positioned OEGMA monomers have side-chains wrap around the main chain to

407   varying extents at different time points of unfolding. Consequently, the wrapping behavior is not

408   a one-size-fits-all process, and sequence effects play an important role to enable the protection

409   mechanism at a given time point. This is analogous to protein PEGylation, where the site of

410   conjugation in a protein also affects the extent of mechanical reinforcement imparted by PEG

411   chains.[50,51] For our RHPs, per the side-chain-based contact maps provided in Figure S11, it may be

412   hypothesized that OEGMA monomers surrounded by MMA monomers are less prone to partake

413   in the proposed protection mechanism *via* side-chain wrapping. Previous analysis has shown that

414   OEGMA monomers in equilibrated RHPs are better solvated when they are surrounded by MMA

415   residues compared to when surrounded by EHMA residues[15], corroborating our observations.

416   Since EHMA is more hydrophobic than MMA, side-chain wrapping around the EHMA residues

417   to minimize water contact is energetically beneficial for the system, suggesting a protection

418   mechanism at play.

419   ***Physicochemical factors affecting RHP unfolding***

420   A variety of physicochemical parameters, including chain length, chemical composition,

421   sequence characteristics, and backbone topology, can influence the RHP unfolding pathway, force

422   curve features, mechanostability, and nonequilibrium unfolding work. Specifically, RHP

423   mechanostability, or the mechanical resistance of RHPs to the applied tensile force, is

424   characterized using peak forces and their distributions. First, on average, RHPs of 50 monomers

425   in length are found to be more mechanically stable than the 20mers (Figure S12). This can be

426   reasoned from the previous conclusion that 50mers typically begin from a state of greater chain

427   compactification due to lower solubility and higher propensity for hydrophobic collapse. As a

428   result of such compactification, the unfolding pathways of 20mers and 50mers also differ. Many

429   20mer RHPs and homopolymers can unfold *via* an Ω-shaped topological intermediate (Figure 5).

430   Since this is common to sequences having different chemical compositions and sequence traits,

431   the Ω-shaped intermediate may have a topological origin given that most compact 20mers

432   investigated initially assume a U- or O-shape, where the 2D projection of an RHP backbone onto

433   any surface gives a U-shape if there is no intersection and an O-shape if there is one intersection.

434   Notably, an unfolding pathway phenomenologically similar to the pathway proposed here has been

435   observed during the mechanical unfolding of biological β-hairpin structures[52,53], despite the fact

436   that specific hydrogen bonding is responsible for stabilizing β-hairpins whereas nonspecific

437   hydrophobic interactions are responsible for stabilizing our RHPs. 50mer RHPs, on the other hand,

438   have more diverse topologies and, as a result, more diverse unfolding behaviors. Previous

439   theoretical analysis on amphiphilic heteropolymer unfolding suggests the existence of a pearl-

440   necklace unfolding intermediate due to favorable solvation in hydrophilic residues and unfavorable

441   solvation in hydrophobic ones.[13,14] However, this is rarely seen in the multicomponent RHPs. When

442   the pearl-necklace unfolded intermediate is observed, we find that the pearl formation is not

443   necessarily due to the unfolding of hydrophilic cluster(s) within the polymer sequence; rather,

444   reduced steric hindrances in MMA segments facilitate unfolding through a linker-like mechanism

445   as discussed in the case study. In addition, we suspect that the solvent-shielding protection

446   mechanism discussed previously can alter the unfolding pathway by modulating the barriers

447   pertinent to the water solvation energetics, thus eliminating the need for a necklace structure during

448   the force-induced globule-coil transition.[54] Therefore, we find that, in addition to hydrophobicity

449   and hydrophilicity of the monomers, their exact chemistry and sterics impact the RHP unfolding

450   response, which would not have been captured by coarse-grained simulations and theories.

451   Our RHPs possess high chemical heterogeneity with lengthy and/or bulky side-chains that prove

452   impactful to their unfolding responses. Since chemical composition, sequence characteristics, and

453   backbone topologies cannot be easily decoupled for our statistically random polymers, these are

454   examined holistically to provide insights into their effects on unfolding and mechanostability. The

455   effect of chemical composition is investigated by examining the monomer content in each chain

456   using pooled data across sequences (Figures S13 and S14). No strong correlations are observed

457   for 20 or 50mer sequences, indicating that chain composition alone cannot dictate the mechanical

458   response of a chemically heterogeneous RHP. One might expect that, as the most prevalent

459   stabilizing interactions in RHPs are EHMA-EHMA hydrophobic attraction, its content would have

460   a high correlation with mechanostability. However, even though PEHMA homopolymer is

461   relatively mechanically stable, having a high fractional content of EHMA in the RHP does not

462   guarantee the same. A weak negative correlation can be observed between SPMA content and

463   RHP mechanostability due to electrostatic repulsions, though RHPs with the same chemical

464   composition (20mer RHP sequences 9 and 13) can produce disparate mechanical responses. These

465   results hint that sequence and/or topological effects may be of more relevance than chemical

466   composition for mechanostability.

467   The work required for unfolding an RHP is calculated as the area under the force curve, with the

468   integral evaluated from initial end-to-end distance to 45 Å for 20mers and 110 Å for 50mers.

469   Unfolding work is rate-dependent for polymeric systems, but can nevertheless provide information

470   on the internal friction in polymeric globules, which in turn reflects the roughness of their

471   conformational energy landscape.[8,55,56] Figure 8 maps the specific unfolding work against the

472   change in specific total SASA upon polymer unfolding for homopolymers and RHPs, where

473   "specific" properties are normalized by the polymer molecular weights. The change in SASA

474 should encompass effects of both molecular weight and overall hydrophilicity, allowing each

475 sequence to be compared. We notice that there are several cases where ΔSASA/MW is negative

476 (Figure 8), all of which come from different RHP unfolding replicates. This can be explained by

477 the amphiphilic nature of OEGMA side-chains as well as the fact that OEGMA is a main

478 determinant of the magnitude of the overall SASA as it has lengthy side-groups. The PEG chains

479 in OEGMA residues can either wrap around the main chain as previously discussed, giving rise to

480 relatively low values of total SASA values, or become fully solvated, giving rise to high SASA.

481 The balance between the two at the start and end of the unfolding trajectory then partly dictates

482 the magnitude of ΔSASA – where some of which can be negative in value. First, comparing 20mers

483 and 50mers, the longer polymers which compactify more require a greater specific unfolding work.

484 In addition, relative to the limits established by the homopolymers, namely PMMA and PEHMA

485 specific unfolding work, the 50mer data also has a tighter distribution. Our chemically

486 heterogeneous 50mer RHPs experience relatively uniform compactification and are more dense

487 compared to 20mers, suggesting that the specific unfolding work correlates well with polymer

488 compactness and molecular weight. This has also been demonstrated on unfolded or disordered

489 proteins that the magnitude of internal friction correlates with protein compactness.[55] Closer

490 examination of the nonequilibrium unfolding work shows that there are minimal trends relating

491 unfolding work to the chemical composition of the polymer chains and corroborate the observation

492 that all of the 50mer RHPs studied have similar extents of internal friction (Figure S15). A weak

493 positive correlation exists for unfolding work and the number of OEGMA monomers in a 20mer

494 RHP. Since OEGMA has long side-chains, giving a brush-like architecture, it will have the greatest

495 contribution to internal friction which in our case would predominantly be due to intramolecular

496 side-chain interactions.

497

498
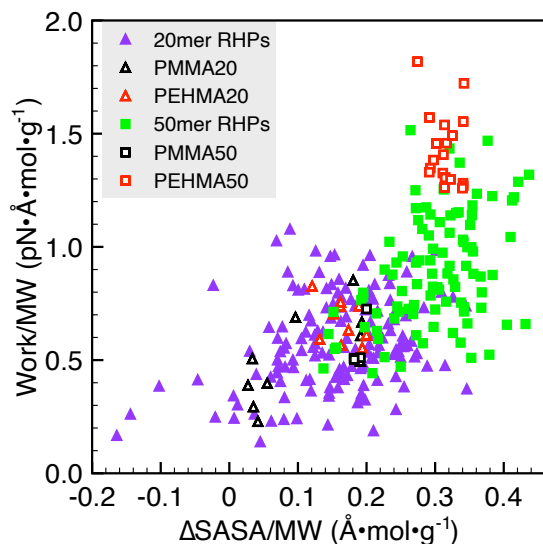
Figure 8. Specific non-equilibrium unfolding work (work / molecular weight MW) for homopolymers and RHPs *versus* the change in specific total SASA (ΔSASA / MW). ΔSASA is calculated by subtracting the average total SASA of the polymer in the first 2 ns of the unfolding simulation from that in the last 2 ns of the simulation. Individual data points are from each unfolding replicate, including five replicates for each sequence of thirty 20mer RHP sequence/conformation, nineteen 50mer RHP sequence/conformation, two PMMA$_{20}$, one PMMA$_{50}$, two PEHMA$_{20}$, and four PEHMA$_{50}$. A similar plot where calculated unfolding work is based on a defined chain extension interval is shown in Figure S16.

507

Examining the effect of sequence characteristics is less obvious for our data, yet postulates can be put forward. Chains with alternating hydrophilic (OEGMA or SPMA) and hydrophobic (MMA or EHMA) monomers were likely to display force curves that are generally increasing in a monotonic fashion without pronounced features (Figure 4). Similarly, sequence effects on the mechanical response of 50mer RHPs can be rationalized on a case-by-case basis, albeit not

26

513 deterministically. RHPs with high SPMA content and SPMA spaced out within a chain result in

514 very mechanically labile unfolding because electrostatic repulsions between anionic groups

515 facilitate the hydration and unfolding of the chain. Yet, there are exceptions, and this is not the

516 case for sequence 5. The destabilizing effect of having a relatively high SPMA content is

517 counteracted by high hydrophobic content, leading to more compact chain morphology upon

518 hydrophobic collapse and giving rise to pronounced peak features. To enable a predictable power

519 for rational design of the multicomponent RHPs, further and more systematic analysis on sequence

520 characteristics is needed. This points to future work on developing statistical models that can be

521 used to assess and quantify sequence traits. Similar analysis has been carried out in protein

522 homology considering the vast number of possible permutations of the amino acid constituents,

523 which can be informative when investigating the RHP systems.[57]

524   Topological design in heteropolymer systems is an emerging topic in macromolecular

525 engineering.[58,59] Our RHPs provide a library of sequences with distinct metastable conformational

526 states stabilized by reversible intramolecular interactions, offering opportunities to decouple

527 sequence and topological effects. We first select two compact 20mer conformers and compare

528 their peak force distributions (Figure S17), noting that different initial equilibrated structures of

529 identical 20mer sequences can have dissimilar mechanical responses to the tensile stimulus. While

530 20mers have backbones that are topologically simple and similar, 50mers have more diverse

531 conformations and topological organizations and can further shed light on how polymer topology

532 affects the single-chain mechanics of RHPs. Four conformations each of the homopolymer

533 PEHMA and of two RHP sequences (sequence 15 and sequence 19) have been investigated. Visual

534 inspection of the different initial conformations reveals that the homopolymers are more spherical

535 in shape – though the exact chain topologies differ for the four conformations, whereas the two

536   heteropolymers in question adopt more varied morphologies (Figure 9). For both homo- and

537   heteropolymers, unique chain topologies result in distinct mechanical responses to forced

538   unfolding (Figure 9). This aligns with previous results on proteins, whose native topology can

539   greatly impact its unfolding behavior, as the initial chain topology restrains the progression of

540   unfolding events that can take place.[60–62] For the heteropolymers, the effect of chain topology is

541   more evident. Structure *2* of sequence 15 has a slightly planar morphology, and the two chain ends

542   point in opposite directions. As a result, mechanical unfolding of this conformation leads to an

543   initial resistance, followed by a drop to near-zero force, indicating nearly spontaneous unfolding

544   behavior at relatively high chain extension. Closer scrutiny of the initial resistance reveals two

545   contributing factors. During initial mechanical perturbance of the polymer, the planar-like

546   morphology deforms laterally and becomes more prolate/ellipsoidal (Figure S18). The internal

547   friction from OEGMA side-chain interactions likely contribute to the initial peak observed in the

548   averaged force curve. A tadpole-like unfolding intermediate, where a globule-shaped head is in

549   coexistence with a stretched chain end[63], is observed at around $t = 30$ ns for this structure but not

550   the other topologies of the same RHP sequence. At around $t = 40$–45 ns, EHMA-EHMA

551   hydrophobic interactions become disrupted to allow further chain extension, after which force

552   drops to a near-zero value as essentially all stabilizing intramolecular interactions have been

553   disrupted, and no further pronounced force peaks are observed (Figures 9B and S18). On the other

554   hand, prolate structures of the heteropolymer (structures *2* and *3*) can display a relatively sustained

555   mechanical resistance over a large range of end-to-end distances (Figure 9). Sequence 19, which

556   is high in negatively-charged SPMA content, is chosen as another RHP for investigating the effect

557   of topology. While two of the native conformations (structures *1* and *3*) unfold easily, mostly

558   attributable to electrostatic repulsion between anions which facilitates unfolding, the remaining

559   two conformations display pronounced force peak features in their unfolding force curves.

560   Therefore, even with high SPMA content, there may exist topologies for which high

561   mechanostability may be achieved. Interestingly, structure *4* of sequence 19 also requires the

562   highest force (285 pN on average, with the highest being 410 pN in one of the replicates) to unfold

563   compared to the different conformers of PEHMA or sequence 15. We hypothesize that, for this

564   topological organization of the backbone, the arrangement of negatively-charged sulfate ions

565   within the SPMA side-chains amplifies the strength of the hydrophobic attraction, similar to

566   previous experimental and simulation results proving the modulation of hydrophobic effect by

567   proximal (*i.e.,* within 1 nm) covalently-attached charged moieties in an ion-specific fashion.[64,65]

568   For this RHP conformation (sequence 19 structure *4*), its unfolding requires the cooperative

569   breaking of multiple types of interactions at approximately the same time, leading to one

570   pronounced force peak at low extension (Figure 9C).

571   Comparing the intramolecular contact evolutions of the unique topological conformations

572   (Figures 9 and S19) offers additional insight. First, both the time-evolution of contact maps and

573   the contact reduction trends are similar between replicates of a specific topology for a given

574   polymer sequence. For the RHPs, this would suggest that, once we have a metastable structure,

575   there exists a generally consistent energetic pathway for unfolding, though small deviations can

576   exist. Secondly, we find that homopolymer unfolding leads to both dissolution and reformation of

577   contacts whereas heteropolymer unfolding is predominantly mediated by the dissolution of contact

578   features. Thus, backbone restructuring is more common in the homopolymer compared to in the

579   heteropolymer upon unfolding, following the mobility trends obtained in previous unbiased

580   simulations.[15] From an enthalpic point of view, monomer-monomer interactions are all identical

581   within homopolymers, whereas heteropolymers have a multitude of possible interactions between

582   the different monomer types. These inter-monomeric potentials lead to a much more textured

583   energy landscape of the evolving RHP conformations since there are now ten unique monomer

584   pairings rather than the single homopolymer self-interaction. Polarity, electrostatics, and

585   hydrophilicity lead EHMA-EHMA and OEGMA-OEGMA associations to be favored while

586   SPMA-SPMA and SPMA-EHMA interactions are avoided. From a topological perspective, all

587   four conformations of PEHMA investigated possess an initial antiparallel topology (contacts

588   forming a line perpendicular to the main diagonal), which then induces an unzipping-type behavior

589   by reconfiguring to a helical-like topology (contacts residing next and parallel to the main

590   diagonal). This unfolding response *via* unzipping is enabled by the high entropic conformational

591   flexibility of the backbone as well as that of the side-chains evidenced by the gradual reduction in

592   intramolecular contacts for homopolymers, while the heteropolymers show more varied contact

593   reduction rates throughout the trajectories (Figure 9). Moreover, force peak occurrences appear to

594   correlate with a rapid reduction in intramolecular contacts, with the magnitude of the force peak

595   being dependent on the nature of monomer-monomer interactions disrupted upon unfolding. There

596   is also greater variability in the contact reduction curve behavior between each topological

597   conformation as well as between replicates of the same conformation for the RHPs compared to

598   the PEHMA homopolymer.

599
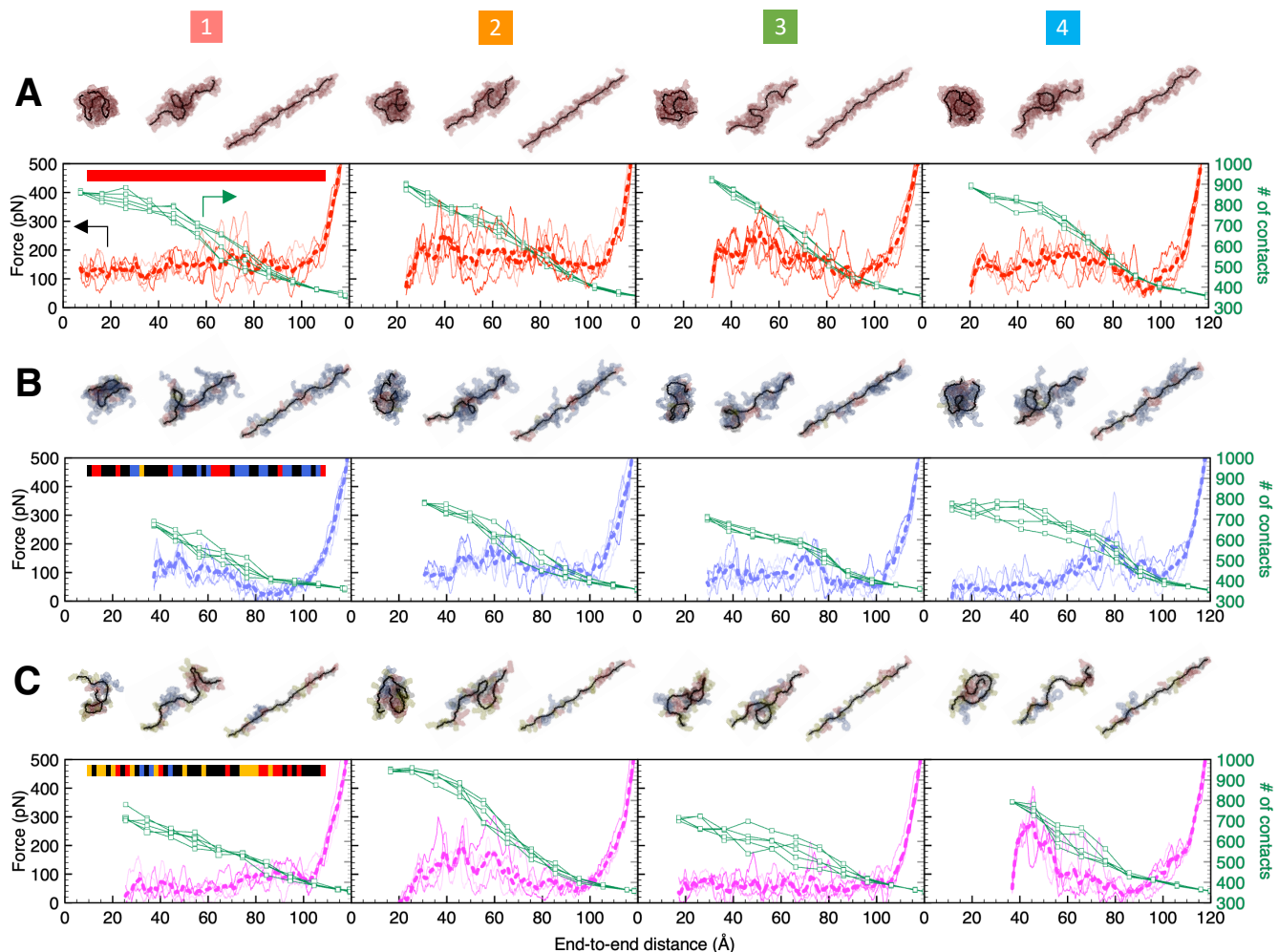
Figure 9. Backbone topology affects RHP unfolding responses. Unfolding force curves of four different starting conformations, numbered 1–4, of (A) homopolymer PEHMA and (B, C) RHP sequence 15 and 19. Superimposed are contact data (in dark green) showing the reduction in the number of intramolecular contacts during RHP unfolding (one curve for each replicate; see Methods for details). Corresponding contact map evolutions and contact reduction curves in a different presentation style can be found in Figure S19.

For further comparison of chemical and topological contributions to unfolding behavior, we compare the dihedral angle dynamics between the different polymer sequences and between

610 conformations. The standard deviation of |dihedral angles| across the entire unfolding trajectory

611 can be used as a proxy for the extent of backbone reconfiguration, allowing identification of

612 mechanically stable regions (*i.e.,* chain segments that undergo minimal transition in all five

613 unfolding replicates) within a polymer chain (Figure S20A–C). Both PEHMA and RHP sequences

614 showed regions that remained mechanically stable from each initial topology. However, in the

615 RHPs, the segments closest to the chain ends offered a disproportionately consistent opportunity

616 for reconfiguration. Further analysis of the chiral nature of the monomers along the sequence

617 revealed that the emergence of mechanically stable segments correlates with alternating chirality

618 in the residues (Figure S20D). Additionally, both intra- and inter-monomeric dihedrals can mediate

619 conformational changes upon mechanical unfolding with no preference of one over the other

620 (Figure S21). This highlights the capability of atomistic MD simulations to capture the high

621 conformational flexibility of the polymer backbone. Overall, our results demonstrate that, for a

622 multicomponent polymeric system with topological heterogeneity, both the backbone

623 conformation and sequence are important factors in affecting the single-chain unfolding response,

624 with topological effects capable of outweighing chemistry or sequence effects.

625 The above analysis highlights the importance of topology in affecting the unfolding response,

626 pathway, and dynamics of single-chain heteropolymer systems. Additionally, topological design

627 can be a viable option to tune the mechanical response of a heteropolymer. In practice, both internal

628 and external confinement strategies can be employed to force single-chain heteropolymers into

629 certain topologies.[59] Internal confinement utilizes intramolecular crosslinking and/or orthogonal

630 chemistry. Perez-Baena *et al*. have used long bifunctional crosslinkers *via* thiol-yne coupling

631 reaction to promote the formation of long-range loops in compactified SCNPs.[66] External

632 confinement refers to physical confinement of the polymers at the nanoscale, consequently altering

633 the configurational sampling space of the system.[39,59] Therefore, synthesis of high concentrations

634 of RHPs within a nanofluidic device with optimized channel geometries may be of interest in

635 future experimental work for directed topological RHP synthesis. Processing conditions can also

636 be coupled to the aforementioned strategies to assist formation of desired topological structures.[67]

637 To gain further understanding of how RHP topological motifs might correlate with force curve

638 features, emerging concepts such as circuit topology and graph theory could be applied[58].

639 Additionally, a greater variety of RHP sequences with various chemistries and characteristics

640 could provide enough data for a rigorous quantitative model, though computational costs of the

641 pulling simulations remain a hurdle. As demonstrated in one RHP (sequence 19), the realization

642 that spatially-defined anions within a fold can modulate the strength of hydrophobic attraction

643 should also promote new research into this area by combining topological control with sequence-

644 defined polymer synthesis. This would allow us to design in structural (in)stabilities for relevant

645 applications for synthetic heteropolymers or SCNPs self-assembled through hydrophobic collapse.

646 **CONCLUSIONS**

647   In summary, this work investigates the structure and single-molecule mechanics of protein-

648 inspired RHPs in water using all-atom simulations. The four-component heterochiral RHPs sample

649 from a broad statistical distribution of metastable conformations, and so do their properties. As a

650 result, their structure-property landscape proves highly complex, and there is no singly defined

651 response to forced unfolding for the RHPs. Nevertheless, our data suggest that the physicochemical

652 parameters of the RHPs, particularly the backbone topology, can be tuned to enable specific

653 unfolding responses, which may be leveraged to mediate specific interactions with

654 biomacromolecules. As the RHP system presented here also belongs to the active field of SCNPs,

655 our findings on the chemical heterogeneity in polymer design, topological organization of the

656 polymer backbone, and the importance of side chain length and bulkiness in modulating polymer

657 behavior may open doors for further research in this area. More generally, this work highlights the

658 necessity of atomistic details in elucidating single-molecule mechanics of multicomponent

659 heteropolymers, revealing phenomena (such as the existence of a dynamic multitude of unfolding

660 pathways as well as the OEGMA wrapping as a protection mechanism) that cannot be easily

661 captured by previously proposed theories. Overall, heteropolymer systems with high chemical and

662 conformational heterogeneity, such as the one presented here, necessitate further exploration.

663 **METHODS**

664 *Unbiased molecular dynamics (MD) simulation details*

665 RHP sequences with degrees of polymerizations of 20 and 50 (referred as 20mers and 50mers,

666 respectively, in this work) were simulated by selecting the first 20 and the first 50 residues of

667 100mer RHPs with target compositions of MMA:OEGMA:EHMA:SPMA in ratios of either

668 50:25:20:5 or 50:5:30:15 by number generated and parameterized per methods in Hilburg *et al*.[15]

669 Annealing protocol initially minimized and equilibrated at 500 K for 40 ns and then ramped down

670 to 300 K over 40 ns in implicit solvent. This was repeated ten times and each resulting structure at

671 300 K was extracted for explicit solvation in a periodic octahedral geometry with approximately

672 40,000 molecules of SPC/E water and potassium counterions (to offset SPMA charges). Each

673 structure was then annealed to 650 K, held for 20 ns, and cooled down to 300 K over 40 ns. The

674 structures were then held at 300 K for 60ns, the latter 40 ns of which were used for analysis. The

675 final frames of these trajectories were then used for unfolding simulations.

676 *Steered molecular dynamics (SMD) simulations*

677 SMD simulations were performed on the obtained equilibrated structures using a constant-

678 velocity protocol in order to mechanically unfold the RHPs in explicit water at 300 K. For all RHP

679 sequences and conformations studied, the two ends are defined to be the backbone C_β atom of the

680 first monomeric unit and the backbone C_α atom of the terminal unit (Figure S2). A biasing potential

681 is applied to the two ends with a force constant of 7.0 kcal mol^{-1} Å^{-2}, pulling the two ends apart at

682 a constant speed of 1.0 Å ns^{-1}. Other parameterizations, including Langevin thermostat and

683 Berendsen barostat, remain identical to those reported in Hilburg *et al.*[15] All 20mer RHPs are

684 stretched until the end-to-end distance reaches 50 Å, and all 50mers are stretched until 120 Å,

685 where there are no apparent interactions between non-adjacent monomers. Five independent

686 replicates initiated with new random velocities were performed for all RHP sequences studied.

687 The choices of simulation parameters have been informed by previous works involving the use of

688 SMD (Table S1).

689 *In silico* stress-relaxation experiments were performed to gain insights into the dissipation of

690 induced tensile stress from the unfolding process of single-chain RHPs. Snapshots of interest were

691 selected at particular time points from throughout the one-stage pulling trajectories and used to

692 obtain the atomic coordinates. Randomized velocities are used to initiate the stress-relaxation

693 simulations. The restraint on the end-to-end distance in SMD is set to be a constant, equivalent to

694 that at which the snapshot was extracted, and RHPs are allowed to relax at that restrained end-to-

695 end distance for 20 ns. For each snapshot, three independent stress-relaxation experiments are

696 reported.

697 ***Analysis***

698 Cpptraj and Pytraj[68] are used to analyze all simulation trajectories as per AMBER19 manual[69],

699 and VMD[70] (Visual Molecular Dynamics) is used for visualization.

700 **Force curves and analysis.** For each unfolding experiment using SMD, the force applied is

701 recorded as a function of the polymer's end-to-end distance. A moving average over 2-Å intervals

702   is calculated to improve signal-to-noise ratios in the force curves. Peak force analysis is done using

703   the SciPy library in Python to characterize the mechanical stability of RHPs and of their

704   homopolymer counterparts. In particular, a feature with peak value greater than 42 pN and a

705   prominence value greater than 28 pN is considered as a peak. For any given sequence, all peaks

706   pooled from the five independent replicates are included in the peak force distribution analysis.

707   Nonequilibrium unfolding work is calculated as the integral of the unfolding force curve evaluated

708   from the initial end-to-end distance to 45 Å for 20mers and 110 Å for 50mers, respectively.

709   **Dihedral angles.** A dihedral angle characterizes bond rotations in a polymer and thus its

710   conformational state. As every four neighboring atoms define a dihedral angle, plotting the

711   dihedral angles along the carbon-carbon backbone of a RHP chain gives a 1D topological

712   fingerprint for that RHP. Dihedral angles are averaged over 2-ns of simulation with standard errors

713   computed, and the absolute value is reported to produce dihedral plots.

714   **Contact analysis.** Contact maps plotting the intramolecular distances of all possible pairs of

715   monomers in a given chain as a two-dimensional matrix have been extensively used in the

716   literature for protein structural analysis. The internal structure of our RHPs and its evolution upon

717   unfolding is used in an analogous fashion. Three types of contact map analyses are performed in

718   this work based on: C_α atoms in the backbone, the center-of-mass of the side-chains, and tail atoms

719   in the side-chains (Figure S2). All contact map data are averaged over 2-ns of simulation

720   trajectories. Contact map data is directly used to determine the number of contacts formed between

721   monomeric residues at a given time (averaged over 2 ns). For 50mers, a contact is considered to

722   be established if the monomer-monomer distance, whether it is C_α-based or side-chain-based, is

723   less than 20 Å. Excluding non-contact entries in a contact matrix and avoiding double-counting,

724   the number of contacts at a given time is thus given by $n_{\text{contacts}} = \frac{n_{\text{values below threshold}} - n_{\text{diagonal}}}{2}$ where

725    $n_{\text{values below threshold}}$ is the number of entries in the contact matrix below the threshold and n_{diagonal}

726   is the number of diagonal entries, *i.e.*, 50 for 50mers.

727   **Solvent-accessible surface area.** Solvent accessible surface area (SASA) of an RHP is the

728   surface area that is exposed to water molecules as calculated using the linear combination of

729   pairwise overlaps algorithm (LCPO) as implemented in AMBER19 (ref. [69]), and all atom

730   contributions from a given RHP molecule are considered for SASA evaluation.

731   **Water shell solvation.** Solvation data provides information on the solvent-accessible regions of

732   RHPs upon unfolding. The normalized first solvation shell (NFSS) is computed as the number of

733   water molecules in the first solvation shell relative to that in a well-solvated monomer of the same

734   type per Hilburg *et al.*[15]

735   *Statistical analysis*

736   ANOVA tests were conducted using Python to ascertain statistical significance (*$p < 0.05$)

737   between sampling distributions.

738

739   **ASSOCIATED CONTENT**

740   **Supporting Information.**

741   The Supporting Information is available free of charge at xxx.

742   RHP sequence schematics. Atom designations. Heterogeneous conformational sampling in

743   RHPs. Additional stress-relaxation results. Unfolding force curves for all RHPs studied.

744   Characterization of independent unfolding replicates. Snapshots showing the unfolding pathway

745   of a 50mer RHP. OEGMA wrapping: snapshots, contact maps, and monomer-monomer

746   separational distances. Peak force distributions. Additional analysis on non-equilibrium unfolding

747 work. Effects of backbone topology: unfolding trajectory snapshots, contact map evolutions, and

748 contact reduction curves. Dihedral dynamics. (PDF)

749   Movie of a 50mer RHP unfolding trajectory. (MOV)

750

751 **AUTHOR INFORMATION**

752 **Corresponding Author**

753 * Alfredo Alexander-Katz – Department of Materials Science and Engineering, Massachusetts

754 Institute of Technology, Cambridge, Massachusetts 02139, United States; Email:

755 aalexand@mit.edu

756 **Authors**

757 Zexiang Han – orcid.org/0000-0002-8968-0860

758 Shayna L. Hilburg – orcid.org/0000-0003-0825-7698

761 **Notes**

762 The authors declare no competing financial interest.

REFERENCES

(1)   Stirnemann, G.; Kang, S. G.; Zhou, R.; Berne, B. J. How Force Unfolding Differs from Chemical Denaturation. *Proc. Natl. Acad. Sci. U. S. A.* **2014**, *111* (9), 3413–3418. DOI: 10.1073/pnas.1400752111

(2)   Marszalek, P. E.; Lu, H.; Li, H.; Carrion-Vazquez, M.; Oberhauser, A. F.; Schulten, K.; Fernandez, J. M. Mechanical Unfolding Intermediates in Titin Modules. *Nature* **1999**, *402* (6757), 100–103. DOI: 10.1038/47083

(3)   Lu, H.; Isralewitz, B.; Krammer, A.; Vogel, V.; Schulten, K. Unfolding of Titin Immunoglobulin Domains by Steered Molecular Dynamics Simulation. *Biophys. J.* **1998**, *75* (2), 662–671. DOI: 10.1016/S0006-3495(98)77556-3

(4)   Gao, M.; Wilmanns, M.; Schulten, K. Steered Molecular Dynamics Studies of Titin I1 Domain Unfolding. *Biophys. J.* **2002**, *83* (6), 3435–3445. DOI: 10.1016/S0006-3495(02)75343-5

(5)   Paramore, S.; Voth, G. A. Examining the Influence of Linkers and Tertiary Structure in the Forced Unfolding of Multiple-Repeat Spectrin Molecules. *Biophys. J.* **2006**, *91* (9), 3436–3445. DOI: 10.1529/biophysj.106.091108

(6)   Lee, G.; Abdi, K.; Jiang, Y.; Michaely, P.; Bennett, V.; Marszalek, P. E. Nanospring Behaviour of Ankyrin Repeats. *Nature* **2006**, *440* (7081), 246–249. DOI: 10.1038/nature04437

(7)   Einert, T. R.; Sing, C. E.; Alexander-Katz, A.; Netz, R. R. Conformational Dynamics and Internal Friction in Homopolymer Globules: Equilibrium vs. Non-Equilibrium Simulations. *Eur. Phys. J. E* **2011**, *34* (12). DOI: 10.1140/epje/i2011-11130-8

(8)   Alexander-Katz, A.; Wada, H.; Netz, R. R. Internal Friction and Nonequilibrium Unfolding of Polymeric Globules. *Phys. Rev. Lett.* **2009**, *103* (2), 1–4. DOI: 10.1103/PhysRevLett.103.028102

(9)   Li, I. T. S.; Walker, G. C. Signature of Hydrophobic Hydration in a Single Polymer. *Proc. Natl. Acad. Sci. U. S. A.* **2011**, *108* (40), 16527–16532. DOI: 10.1073/pnas.1105450108

(10)   Chung, J.; Kushner, A. M.; Weisman, A. C.; Guan, Z. Direct Correlation of Single-Molecule Properties with Bulk Mechanical Performance for the Biomimetic Design of Polymers. *Nat. Mater.* **2014**, *13* (11), 1055–1062. DOI: 10.1038/NMAT4090

(11)   Hosono, N.; Kushner, A. M.; Chung, J.; Palmans, A. R. A.; Guan, Z.; Meijer, E. W. Forced Unfolding of Single-Chain Polymeric Nanoparticles. *J. Am. Chem. Soc.* **2015**, *137* (21),

6880–6888. DOI: 10.1021/jacs.5b02967

(12) Levy, A.; Feinstein, R.; Diesendruck, C. E. Mechanical Unfolding and Thermal Refolding of Single-Chain Nanoparticles Using Ligand-Metal Bonds. *J. Am. Chem. Soc.* **2019**, *141* (18), 7256–7260. DOI: 10.1021/jacs.9b01960

(13) Geissler, P. L.; Shakhnovich, E. I. Reversible Stretching of Random Heteropolymers. *Phys. Rev. E - Stat. Physics, Plasmas, Fluids, Relat. Interdiscip. Top.* **2002**, *65* (5), 4. DOI: 10.1103/PhysRevE.65.056110

(14) Geissler, P. L.; Shakhnovich, E. I. Mechanical Response of Random Heteropolymers. *Macromolecules* **2002**, *35* (11), 4429–4436. DOI: 10.1021/ma012008e

(15) Hilburg, S. L.; Ruan, Z.; Xu, T.; Alexander-Katz, A. Behavior of Protein-Inspired Synthetic Random Heteropolymers. *Macromolecules* **2020**, *53* (21), 9187–9199. DOI: 10.1021/acs.macromol.0c01886

(16) Bustamante, C.; Bustamante, C.; Alexander, L.; MacIuba, K.; Kaiser, C. M. Single-Molecule Studies of Protein Folding with Optical Tweezers. *Annu. Rev. Biochem.* **2020**, *89*, 443–470. DOI: 10.1146/annurev-biochem-013118-111442

(17) Neuman, K. C.; Nagy, A. Single-Molecule Force Spectroscopy: Optical Tweezers, Magnetic Tweezers and Atomic Force Microscopy. *Nat. Methods* **2008**, *5* (6), 491–505. DOI: 10.1038/nmeth.1218

(18) Han, Z.; Porter, A. E. In Situ Electron Microscopy of Complex Biological and Nanoscale Systems: Challenges and Opportunities. *Front. Nanotechnol.* **2020**, *2*. DOI: 10.3389/fnano.2020.606253

(19) Moerner, W. E. New Directions in Single-Molecule Imaging and Analysis. *Proc. Natl. Acad. Sci. U. S. A.* **2007**, *104* (31), 12596–12602. DOI: 10.1073/pnas.0610081104

(20) Milles, L. F.; Schulten, K.; Gaub, H. E.; Bernardi, R. C. Molecular Mechanism of Extreme Mechanostability in a Pathogen Adhesin. *Science* **2018**, *359* (6383), 1527–1533. DOI: 10.1126/science.aar2094

(21) Bernardi, R. C.; Durner, E.; Schoeler, C.; Malinowska, K. H.; Carvalho, B. G.; Bayer, E. A.; Luthey-Schulten, Z.; Gaub, H. E.; Nash, M. A. Mechanisms of Nanonewton Mechanostability in a Protein Complex Revealed by Molecular Dynamics Simulations and Single-Molecule Force Spectroscopy. *J. Am. Chem. Soc.* **2019**, *141* (37), 14752–14763. DOI: 10.1021/jacs.9b06776

(22) Brockwell, D. J.; Paci, E.; Zinober, R. C.; Beddard, G. S.; Olmsted, P. D.; Smith, D. A.; Perham, R. N.; Radford, S. E. Pulling Geometry Defines the Mechanical Resistance of a β-Sheet Protein. *Nat. Struct. Biol.* **2003**, *10* (9), 731–737. DOI: 10.1038/nsb968

834   (23)   Deshmukh, S. A.; Li, Z.; Kamath, G.; Suthar, K. J.; Sankaranarayanan, S. K. R. S.; Mancini,
835   D. C. Atomistic Insights into Solvation Dynamics and Conformational Transformation in
836   Thermo-Sensitive and Non-Thermo-Sensitive Oligomers. *Polymer (Guildf)* **2013**, *54* (1),
837   210–222. DOI: 10.1016/j.polymer.2012.11.009

838   (24)   Imai, S.; Hirai, Y.; Nagao, C.; Sawamoto, M.; Terashima, T. Programmed Self-Assembly
839   Systems of Amphiphilic Random Copolymers into Size-Controlled and Thermoresponsive
840   Micelles in Water. *Macromolecules* **2018**, 51, 398−409. DOI:
841   10.1021/acs.macromol.7b01918

842   (25)   Xu, Z.; Sun, Y.; Weber, J. K.; Cao, Y.; Wang, W.; Jasinski, D.; Guo, P.; Zhou, R.; Li, J.
843   Directional Mechanical Stability of Bacteriophage Φ29 Motor's 3WJ-PRNA: Extraordinary
844   Robustness along Portal Axis. *Sci. Adv.* **2017**, *3* (5), 2–10. DOI: 10.1126/sciadv.1601684

845   (26)   Chen, W.; Lou, J.; Hsin, J.; Schulten, K.; Harvey, S. C.; Zhu, C. Molecular Dynamics
846   Simulations of Forced Unbending of Integrin AVβ3. *PLoS Comput. Biol.* **2011**, *7* (2). DOI:
847   10.1371/journal.pcbi.1001086

848   (27)   Bergues-Pupo, A. E.; Arias-Gonzalez, J. R.; Morón, M. C.; Fiasconaro, A.; Falo, F. Role of
849   the Central Cations in the Mechanical Unfolding of DNA and RNA G-Quadruplexes.
850   *Nucleic Acids Res.* **2015**, *43* (15), 7638–7647. DOI: 10.1093/nar/gkv690

851   (28)   Gao, M.; Craig, D.; Lequin, O.; Campbell, I. D.; Vogel, V.; Schulten, K. Structure and
852   Functional Significance of Mechanically Unfolded Fibronectin Type III1 Intermediates.
853   *Proc. Natl. Acad. Sci. U. S. A.* **2003**, *100* (25), 14784–14789. DOI:
854   10.1073/pnas.2334390100

855   (29)   Guzmán, D. L.; Roland, J. T.; Keer, H.; Kong, Y. P.; Ritz, T.; Yee, A.; Guan, Z. Using
856   Steered Molecular Dynamics Simulations and Single-Molecule Force Spectroscopy to
857   Guide the Rational Design of Biomimetic Modular Polymeric Materials. *Polymer (Guildf).*
858   **2008**, *49* (18), 3892–3901. DOI: 10.1016/j.polymer.2008.06.047.

859   (30)   Ozer, G.; Valecv, E. F.; Quirt, S.; Hernandez, R. Adaptive Steered Molecular Dynamics of
860   the Long-Distance Unfolding of Neuropeptide Y. *J. Chem. Theory Comput.* **2010**, *6* (10),
861   3026–3038. DOI: 10.1021/ct100320g

862   (31)   Lu, H.; Schulten, K. Steered Molecular Dynamics Simulations of Force-Induced Protein
863   Domain Unfolding. *Proteins Struct. Funct. Genet.* **1999**, *35* (4), 453–463.

864   (32)   Rico, F.; Gonzalez, L.; Casuso, I.; Puig-Vidal, M.; Scheuring, S. High-Speed Force
865   Spectroscopy Unfolds Titin at the Velocity of Molecular Dynamics Simulations. *Science*
866   **2013**, *342* (6159), 741–743. DOI: 10.1126/science.1239764

867   (33)   Panganiban, B.; Qiao, B.; Jiang, T.; DelRe, C.; Obadia, M. M.; Nguyen, T. D.; Smith, A.
868   A. A.; Hall, A.; Sit, I.; Crosby, M. G.; Dennis, P. B.; Drockenmuller, E.; De La Cruz, M.

O.; Xu, T. Random Heteropolymers Preserve Protein Function in Foreign Environments. *Science* **2018**, *359* (6381), 1239–1243. DOI: 10.1126/science.aao0335

(34)   Delre, C.; Huang, C.; Li, T.; Dennis, P.; Drockenmuller, E.; Xu, T. Reusable Enzymatic Fiber Mats for Neurotoxin Remediation in Water. *ACS Appl. Mater. Interfaces* **2018**, *10* (51), 44216–44220. DOI: 10.1021/acsami.8b18484

(35)   Jiang, T.; Hall, A.; Eres, M.; Hemmatian, Z.; Qiao, B.; Zhou, Y.; Ruan, Z.; Couse, A. D.; Heller, W. T.; Huang, H.; de la Cruz, M. O.; Rolandi, M.; Xu, T. Single-Chain Heteropolymers Transport Protons Selectively and Rapidly. *Nature* **2020**, *577* (7789), 216–220. DOI: 10.1038/s41586-019-1881-0

(36)   DelRe, C.; Jiang, Y.; Kang, P.; Kwon, J.; Hall, A.; Jayapurna, I.; Ruan, Z.; Ma, L.; Zolkin, K.; Li, T.; Scown, C. D.; Ritchie, R. O.; Russell, T. P.; Xu, T. Near-Complete Depolymerization of Polyesters with Nano-Dispersed Enzymes. *Nature* **2021**, *592* (7855), 558–563. DOI: 10.1038/s41586-021-03408-3

(37)   Mishra, A.; Panwar, A. S.; Chakrabarti, B. Equilibrium Morphologies and Force Extension Behavior for Polymers with Hydrophobic Patches: Role of Quenched Disorder. *Macromol. Theory Simulations* **2014**, *23* (4), 266–278. DOI: 10.1002/mats.201300154

(38)   Baul, U.; Chakraborty, D.; Mugnai, M. L.; Straub, J. E.; Thirumalai, D. Sequence Effects on Size, Shape, and Structural Heterogeneity in Intrinsically Disordered Proteins. *J. Phys. Chem. B* **2019**, *123* (16), 3462–3474. DOI: 10.1021/acs.jpcb.9b02575

(39)   Verde-Sesto, E.; Arbe, A.; Moreno, A. J.; Cangialosi, D.; Alegría, A.; Colmenero, J.; Pomposo, J. A. Single-Chain Nanoparticles: Opportunities Provided by Internal and External Confinement. *Mater. Horizons* **2020**, *7* (9), 2292–2313. DOI: 10.1039/d0mh00846j

(40)   Dobrynin, A. V.; Rubinstein, M. Hydrophobically Modified Polyelectrolytes in Dilute Salt-Free Solutions. *Macromolecules* **2000**, *33* (21), 8097–8105. DOI: 10.1021/ma000761m

(41)   Müller-Späth, S.; Soranno, A.; Hirschfeld, V.; Hofmann, H.; Rüegger, S.; Reymond, L.; Nettels, D.; Schuler, B. Charge Interactions Can Dominate the Dimensions of Intrinsically Disordered Proteins. *Proc. Natl. Acad. Sci. U. S. A.* **2010**, *107* (33), 14609–14614. DOI: 10.1073/pnas.1001743107

(42)   Samatha, P.; Krishnamurti, N. Study on Polymerization of Methyl Methacrylate in Water-Solvent Mixtures. *J. Appl. Polym. Sci.* **1997**, *66* (7), 1419–1423.

(43)   Baysal, B. M.; Karasz, F. E. Coil-Globule Collapse in Flexible Macromolecules. *Macromol. Theory Simulations* **2003**, *12* (9), 627–646. DOI: 10.1002/mats.200350028

(44)   Hyeon, C.; Thirumalai, D. Mechanical Unfolding of RNA: From Hairpins to Structures with

903   Internal Multiloops. *Biophys. J.* **2007**, *92* (3), 731–743. DOI: 10.1529/biophysj.106.093062

904 (45) Liu, M.; Leroux, J. C.; Gauthier, M. A. Conformation-Function Relationships for the Comb-
905   Shaped Polymer POEGMA. *Prog. Polym. Sci.* **2015**, *48*, 111–121. DOI:
906   10.1016/j.progpolymsci.2015.03.001

907 (46) Yadavalli, N. S.; Borodinov, N.; Choudhury, C. K.; Quiñones-Ruiz, T.; Laradji, A. M.; Tu,
908   S.; Lednev, I. K.; Kuksenok, O.; Luzinov, I.; Minko, S. Thermal Stabilization of Enzymes
909   with Molecular Brushes. *ACS Catal.* **2017**, *7* (12), 8675–8684. DOI:
910   10.1021/acscatal.7b03138

911 (47) Lee, P.; Towslee, J.; Maia, J.; Pokorski, J. PEGylation to Improve Protein Stability during
912   Melt Processing. *Macromol. Biosci.* **2015**, *15* (10), 1332–1337. DOI:
913   10.1002/mabi.201500143

914 (48) Kaupbayeva, B.; Boye, S.; Munasinghe, A.; Murata, H.; Matyjaszewski, K.; Lederer, A.;
915   Colina, C. M.; Russell, A. J. Molecular Dynamics-Guided Design of a Functional Protein–
916   ATRP Conjugate That Eliminates Protein–Protein Interactions. *Bioconjug. Chem.* **2021**.
917   DOI: acs.bioconjchem.1c00098

918 (49) Debenedictis, E. P.; Hamed, E.; Keten, S. Mechanical Reinforcement of Proteins with
919   Polymer Conjugation. *ACS Nano* **2016**, *10* (2), 2259–2267. DOI: 10.1021/acsnano.5b06917

920 (50) Lawrence, P. B.; Price, J. L. How PEGylation Influences Protein Conformational Stability.
921   *Curr. Opin. Chem. Biol.* **2016**, *34*, 88–94. DOI: 10.1016/j.cbpa.2016.08.006

922 (51) Wilding, K. M.; Smith, A. K.; Wilkerson, J. W.; Bush, D. B.; Knotts, T. A.; Bundy, B. C.
923   The Locational Impact of Site-Specific PEGylation: Streamlined Screening with Cell-Free
924   Protein Expression and Coarse-Grain Simulation. *ACS Synth. Biol.* **2018**, *7* (2), 510–521.
925   DOI: 10.1021/acssynbio.7b00316

926 (52) Bryant, Z.; Pande, V. S.; Rokhsar, D. S. Mechanical Unfolding of a β-Hairpin Using
927   Molecular Dynamics. *Biophys. J.* **2000**, *78* (2), 584–589. DOI: 10.1016/S0006-
928   3495(00)76618-5

929 (53) Hyeon, C.; Dima, R. I.; Thirumalai, D. Pathways and Kinetic Barriers in Mechanical
930   Unfolding and Refolding of RNA and Proteins. *Structure* **2006**, *14* (11), 1633–1645. DOI:
931   10.1016/j.str.2006.09.002

932 (54) Rodriguez-Larrea, D.; Ibarra-Molero, B.; Sanchez-Ruiz, J. M. Energetic and Structural
933   Consequences of Desolvation/Solvation Barriers to Protein Folding/Unfolding Assessed
934   from Experimental Unfolding Rates. *Biophys. J.* **2006**, *91* (5), 48–50. DOI:
935   10.1529/biophysj.106.087932

936 (55) Soranno, A.; Buchli, B.; Nettels, D.; Cheng, R. R.; Müller-Späth, S.; Pfeil, S. H.; Hoffmann,

A.; Lipman, E. A.; Makarov, D. E.; Schuler, B. Quantifying Internal Friction in Unfolded and Intrinsically Disordered Proteins with Single-Molecule Spectroscopy. *Proc. Natl. Acad. Sci. U. S. A.* **2012**, *109* (44), 17800–17806. DOI: 10.1073/pnas.1117368109

(56) Zheng, W.; Hofmann, H.; Schuler, B.; Best, R. B. Origin of Internal Friction in Disordered Proteins Depends on Solvent Quality. *J. Phys. Chem. B* **2018**, *122* (49), 11478–11487. DOI: 10.1021/acs.jpcb.8b07425

(57) Brendel, V.; Bucher, P.; Nourbakhsh, I. R.; Blaisdell, B. E.; Karlin, S. Methods and Algorithms for Statistical Analysis of Protein Sequences. *Proc. Natl. Acad. Sci. U. S. A.* **1992**, *89* (6), 2002–2006. DOI: 10.1073/pnas.89.6.2002

(58) Scalvini, B.; Sheikhhassani, V.; Woodard, J.; Aupič, J.; Dame, R. T.; Jerala, R.; Mashaghi, A. Topology of Folded Molecular Chains: From Single Biomolecules to Engineered Origami. *Trends Chem.* **2020**, *2* (7), 609–622. DOI: 10.1016/j.trechm.2020.04.009

(59) Heidari, M.; Heidari, M.; Schiessel, H.; Mashaghi, A. Circuit Topology Analysis of Polymer Folding Reactions. *ACS Cent. Sci.* **2020**, *6* (6), 839–847. DOI: 10.1021/acscentsci.0c00308

(60) Shank, E. A.; Cecconi, C.; Dill, J. W.; Marqusee, S.; Bustamante, C. The Folding Cooperativity of a Protein Is Controlled by Its Chain Topology. *Nature* **2010**, *465* (7298), 637–640. DOI: 10.1038/nature09021

(61) Paci, E.; Karplus, M. Unfolding Proteins by External Forces and Temperature: The Importance of Topology and Energetics. *Proc. Natl. Acad. Sci. U. S. A.* **2000**, *97* (12), 6521–6526. DOI: 10.1073/pnas.100124597

(62) Klimov, D. K.; Thirumalai, D. Native Topology Determines Force-Induced Unfolding Pathways in Globular Proteins. *Proc. Natl. Acad. Sci. U. S. A.* **2000**, *97* (13), 7254–7259. DOI: 10.1073/pnas.97.13.7254

(63) Polotsky, A. A.; Charlaganov, M. I.; Leermakers, F. A. M.; Daoud, M.; Borisov, O. V.; Birshtein, T. M. Mechanical Unfolding of a Homopolymer Globule Studied by Self-Consistent Field Modeling. *Macromolecules* **2009**, *42* (14), 5360–5371. DOI: 10.1021/ma9004742

(64) Ma, C. D.; Wang, C.; Acevedo-Vélez, C.; Gellman, S. H.; Abbott, N. L. Modulation of Hydrophobic Interactions by Proximally Immobilized Ions. *Nature* **2015**, *517* (7534), 347–350. DOI: 10.1038/nature14018

(65) Huang, K.; Gast, S.; Ma, C. D.; Abbott, N. L.; Szlufarska, I. Comparison between Free and Immobilized Ion Effects on Hydrophobic Interactions: A Molecular Dynamics Study. *J. Phys. Chem. B* **2015**, *119* (41), 13152–13159. DOI: 10.1021/acs.jpcb.5b05220

971 (66) Perez-Baena, I.; Asenjo-Sanz, I.; Arbe, A.; Moreno, A. J.; Lo Verso, F.; Colmenero, J.;
972 Pomposo, J. A. Efficient Route to Compact Single-Chain Nanoparticles: Photoactivated
973 Synthesis via Thiol-Yne Coupling Reaction. *Macromolecules* **2014**, *47* (23), 8270–8280.
974 DOI: 10.1021/ma5017133

975 (67) Formanek, M.; Moreno, A. J. Effects of Precursor Topology and Synthesis under Crowding
976 Conditions on the Structure of Single-Chain Polymer Nanoparticles. *Soft Matter* **2017**, *13*
977 (37), 6430–6438. DOI: 10.1039/c7sm01547j

978 (68) Roe, D. R.; Cheatham, T. E. PTRAJ and CPPTRAJ: Software for Processing and Analysis
979 of Molecular Dynamics Trajectory Data. *J. Chem. Theory Comput.* **2013**. DOI:
980 10.1021/ct400341p

981 (69) D.A. Case, I.Y. Ben-Shalom, S.R. Brozell, D.S. Cerutti, T.E. Cheatham, III, V.W.D.
982 Cruzeiro, T.A. Darden, R.E. Duke, D. Ghoreishi, G. Giambasu, T. Giese, M.K. Gilson, H.
983 Gohlke, A.W. Goetz, D. Greene, R Harris, N. Homeyer, Y. Huang, S. Izadi, A. Kovalenko,
984 R. Krasny, T. Kurtzman, T.S. Lee, S. LeGrand, P. Li, C. Lin, J. Liu, T. Luchko, R. Luo, V.
985 Man, D.J. Mermelstein, K.M. Merz, Y. Miao, G. Monard, C. Nguyen, H. Nguyen, A.
986 Onufriev, F. Pan, R. Qi, D.R. Roe, A. Roitberg, C. Sagui, S. Schott-Verdugo, J. Shen, C.L.
987 Simmerling, J. Smith, J. Swails, R.C. Walker, J. Wang, H. Wei, L. Wilson, R.M. Wolf, X.
988 Wu, L. Xiao, Y. Xiong, D.M. York and P.A. Kollman. AMBER 2019, University of
989 California, San Francisco. **2019**.

990 (70) Humphrey, W.; Dalke, A.; Schulten, K. Sartorius Products. *J. Mol. Graph.* **1996**, *14*
991 (October 1995), 33–38.